EDGE ARTICLE

Check for updates

Destructive quantum interference in heterocyclic alkanes: the search for ultra-short molecular insulators†

Boyuan Zhang, ‡[a] Marc H. Garner, ‡[b] Liang Li, [c] Luis M. Campos, [c] Gemma C. Solomon *[b] and Latha Venkataraman *[ac]

Designing highly insulating sub-nanometer molecules is difficult because tunneling conductance increases exponentially with decreasing molecular length. This challenge is further enhanced by the fact that most molecules cannot achieve full conductance suppression with destructive quantum interference. Here, we present results for a series of small saturated heterocyclic alkanes where we show that conductance is suppressed due to destructive interference. Using the STM-BJ technique and density functional theory calculations, we confirm that their single-molecule junction conductance is lower than analogous alkanes of similar length. We rationalize the suppression of conductance in the junctions through analysis of the computed ballistic current density. We find there are highly symmetric ring currents, which reverse direction at the antiresonance in the Landauer transmission near the Fermi energy. This pattern has not been seen in earlier studies of larger bicyclic systems exhibiting interference effects and constitutes clear-cut evidence of destructive σ-interference. The finding of heterocyclic alkanes with destructive quantum interference charts a pathway for chemical design of short molecular insulators using organic molecules.

Introduction

Designing and measuring sub-nanometer molecular insulators constitutes a fundamental challenge. Current mediated by coherent tunneling increases exponentially with decreasing molecular length.[1,2] Consequently, even molecules with a large HOMO–LUMO gap will not be effective insulators if they are very short. A different route to creating highly insulating molecules is to use molecules with destructive quantum interference effects, which can effectively suppress the coherent single-molecule conductance in the low-bias regime.[3] This effect has been demonstrated in a range of π-conjugated organic molecules[4–8] and in saturated σ-conjugated silanes.[9–12] Saturated molecules with destructive interference in the σ-system have particularly low conductance, as there is no π-channel and transmission through the σ-channel is suppressed.[13–17] This opens a potential avenue for using molecules with destructive σ-

interference as molecular insulators. However, the potential has been limited to date by the restrictive structural requirements for the molecules in which the effect appears.[18–20]

Destructive σ-interference has been demonstrated experimentally in cyclic and bicyclic permethylated silanes,[11,12] and computationally in permethylated alkanes.[10] These molecules have a backbone that is constrained to a cisoid dihedral angle, *i.e.*, one that is approaching 0°.[9,11,21] Alkanes with gauche defects have been accessed experimentally and assessed computationally,[22–27] but the suppression of the conductance is modest. This is presumably due of lack of methyl substituents in the systems that have been examined.[10,28] However, permethylated cyclic and bicyclic alkanes are not synthetically accessible. If the destructive σ-interference effect is to benefit from the broad range of complex molecules available through modern organic synthesis, different classes of saturated systems with the effect need to be explored.

In this article, we examine the single-molecule junction properties of saturated heterocyclic cyclohexane derivates, 1,4-**dithiane**, 1,4-**piperazine** and 1,4-diazabicyclo[2.2.2]octane, **C222-diaza**, also known as DABCO, shown in Scheme 1. These molecules all have molecular length below 5 Å, and thus constitute some of the shortest that can be measured in Au–molecule–Au junctions. Unlike previously explored non-methylated alkanes and methylthiomethyl-functionalized cyclohexanes, we find that these heterocyclic alkanes show

[a]*Department of Applied Physics and Applied Mathematics, Columbia University, New York, New York 10027, USA. E-mail: lv2117@columbia.edu*

[b]*Nano-Science Center and Department of Chemistry, University of Copenhagen, Universitetsparken 5, 2100 Copenhagen Ø, Denmark. E-mail: gsolomon@chem.ku.dk*

[c]*Department of Chemistry, Columbia University, New York, New York 10027, USA*

† Electronic supplementary information (ESI) available: STM-break junction experiment details, conformational analysis, computational details and additional figures. See DOI: 10.1039/d1sc02287c

‡ B. Z. and M. H. G. contributed equally to this work.

Scheme 1 Structures of the Cn-NH$_2$, piperazine, C222-diaza, Cn-SMe, dithiane, and C222-SMe.

significant suppression of conductance due to destructive quantum interference in the σ-system.

Results

Piperazine, **C222-diaza**, and **dithiane** are structurally similar to previously explored silanes[12] exhibiting destructive σ-interference, with the dihedral angles across the cyclic and bicyclic motifs inherently constrained. For **piperazine** and **dithiane** in their dominant chair conformations, these dihedral angles (N–C–C–N and S–C–C–S) are 52° and 67°, respectively. In **C222-diaza** the N–C–C–N dihedral angles are close to 0°. All three systems differ from previous σ-interference systems[10] by the absence of methyl substituents. Furthermore, the molecules studied here are much shorter making them possible insulators over an ultra-short length scale.

Piperazine and C222-diaza

We measure the single-molecule junction conductance of **piperazine** and **C222-diaza** using the scanning tunnelling microscope-based break-junction technique (STM-BJ). We show logarithmically binned two-dimensional (2D) conductance histograms generated from these measurements in Fig. 1a and b. In the STM-BJ technique, single molecule measurements are done by trapping the target molecule between Au electrodes after forming and elongating a single Au atom contact. The conductance feature between 10^{-2} and 10^{-3} G_0 in the 2D histograms between 0 and 0.2 nm displacement correspond to the molecular junction and indicate that these junctions have plateau lengths that extend to about 0.2 nm. Consistent with previous studies, the molecular junction plateau lengths are systematically shorter than the molecular backbone length by roughly 5–8 Å.[29] The tension that the Au-contact is under during the elongation process will cause the relaxation of the electrodes when the Au-contact ruptures, making it difficult to have every junction elongated by the backbone length. Additionally, we cannot assume that every junction forms with the molecule exactly parallel to the pulling direction. Taking such effects into account, both molecules form junctions at short electrode displacement in accordance with their short molecular length. The corresponding one-dimensional (1D) conductance histograms are shown in Fig. 1c, along with that of their linear alkane counterpart ethylenediamine (**C2-NH$_2$**). We determine their junction conductance values by fitting Gaussian functions to
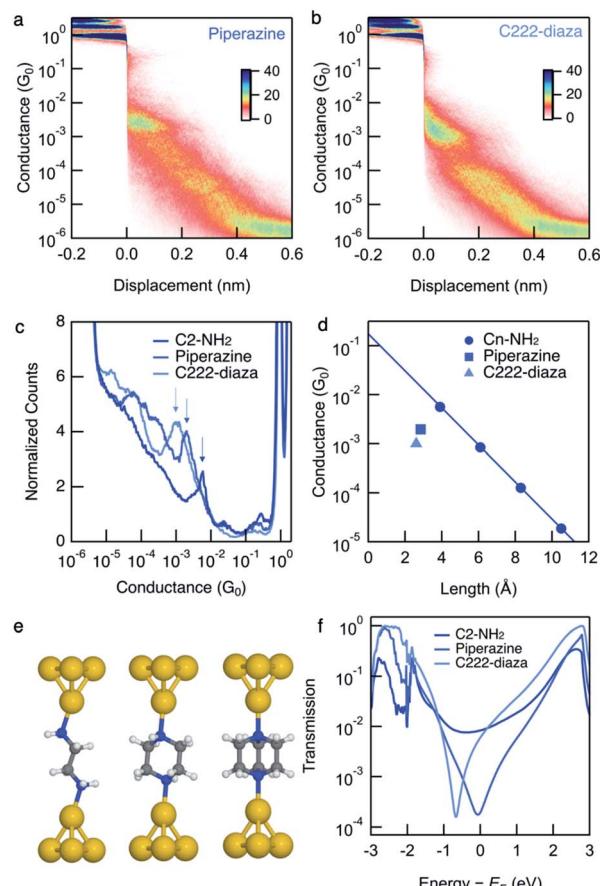
Fig. 1 Logarithmically binned 2D histograms of conductance traces measured with (a) **piperazine** and (b) **C222-diaza**, compiled from 3000–5000 traces without any data selection. (c) Logarithmically binned 1D histograms of conductance traces measured with **C2-NH$_2$**, **piperazine** and **C222-diaza**, compiled from 3000–5000 traces without any data selection. (d) Measured conductance values (histogram peaks) plotted against the molecular length (N–N and is obtained from DFT-optimized structure). **Piperazine**, **C222-diaza** and **dithiane** are below the respective fit conductance decay line for the alkane. See Fig. S1† for raw data. (e) Optimized Au–molecule–Au junction structures of **C2-NH$_2$**, **piperazine**, and **C222-diaza**. (f) Calculated transmissions of Au–molecule–Au junctions plotted against energy relative to Fermi energy, showing anti-resonance around Fermi energy for **piperazine** and **C222-diaza**.

these peaks. The conductance values are centered at 9.5×10^{-4} G_0 and 1.9×10^{-3} G_0 for **C222-diaza** and **piperazine**, respectively, lower than that of **C2-NH$_2$** (5.6×10^{-3} G_0). We note that these histograms represent both the spread in conductance and most frequently measured values.

We compare these experimental conductances with those of amine-terminated linear alkanes. Their experimental single-molecule conductance is plotted against N–N distances obtained from DFT calculations in Fig. 1d. The conductance of the alkane series decays exponentially with increasing length, thereby exhibiting linear decay on a semi-log plot as shown in Fig. 1d. **Piperazine** and **C222-diaza** are both shorter than **C2-NH$_2$** while having the same number of equivalent atoms. Their conductances are below the line of the alkane series, indicating

that they are more insulating than an alkane of the same N–N length.

The amine-terminated alkanes we used to plot the conductance decay line in Fig. 1d are primary amines, while the linkers of **piperazine** are secondary amines and those of **C222-diaza** are tertiary amines. To further validate that the insulating trends of **piperazine** and **C222-diaza** are independent of binding groups, we measure the conductance of secondary and tertiary amine-terminated linear alkanes to understand if the different N linkers account for this reduced conductance. Fig. S2† shows the conductance histogram for a butane backbone with NH_2, $NH-CH_3$ and $N-(CH_3)_2$ linkers where we can see that there is almost no discernible difference among these three indicating that methyl groups on the terminal amine do not alter junction conductance. We can thus conclude that **piperazine** and **C222-diaza** are more insulating than their linear alkane counterparts of the same length, regardless of the structure of the terminal N. We therefore hypothesize that σ-interference in cyclic and bicyclic moiety of **piperazine** and **C222-diaza** can suppress their conductance compared with linear alkanes.

We compute the Landauer transmission of the fully extended Au–molecule–Au junctions visualised in Fig. 1e. Piperazine has conformational freedom, but only conformations where the nitrogen lone-pairs are in equatorial positions appear to be long enough to form junctions in room temperature experiments considering the gap that opens after the gold point-contact is ruptured.[29] Transmission of the shorter junctions are discussed in ESI† part 3. Plotted in Fig. 1f, the transmission of **piperazine** and **C222-diaza** is significantly suppressed in an energy range close to the Fermi energy compared to **C2-NH2**. **Piperazine** and **C222-diaza** both have an antiresonance (dip) close to the Fermi energy in these calculations, which is a signature of destructive quantum interference. We note that the exact energetic position of the antiresonance cannot be exactly predicted due to the quantitative limitations of DFT.[30] The antiresonance is in the vicinity of the Fermi energy in both cases and will affect the single-molecule conductance when a bias-window is opened.

Dithiane

Conductance data obtained from measurements of **dithiane** are shown in Fig. 2a and c. **Dithiane** has well-defined junction geometry that is very similar to –SMe binding motives.[31,32] **Dithiane** has two peaks in the 1D histogram which can be identified as junctions of two different lengths from the 2D histogram. **Dithiane** primarily adapts a chair conformation, which has sulfur lone-pairs available for bonding with the Au electrodes in equatorial and axial positions as illustrated in Fig. 2b. Based on the calculation results shown in Fig. S7,† we attribute the higher-conducting and shorter junction to molecular conformations where the Au is bound either in an axial–axial configuration or axial–equatorial configuration as both of these junctions have roughly the same length and calculated transmission. The shorter junction conformations of SMe-functionalized alkanes were measured in a previous study,[31] where it was found that these also have higher
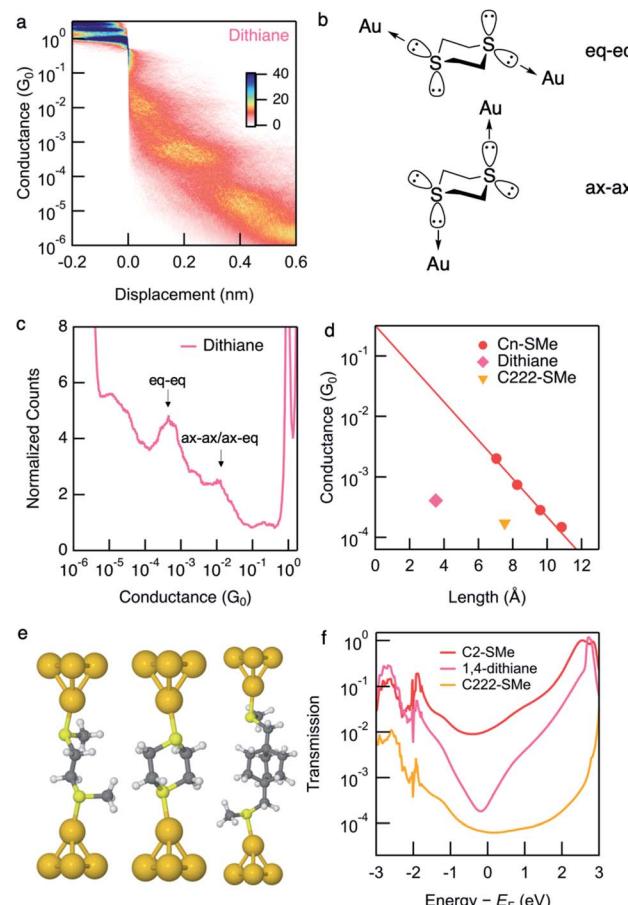
Fig. 2 (a) Logarithmically binned 2D histograms of conductance traces measured with **dithiane** compiled from 3000 traces without any data selection. (b) **Dithiane** structure showing the two S-lone pairs with equatorial–equatorial and axial–axial configurations. (c) Logarithmically binned 1D histograms of conductance traces used to generate panel (a). (d) Measured conductance values (histogram peaks) plotted against the molecular length (S–S length obtained from DFT-optimized structure). Values for linear alkanes are also shown. Conductance values for **C*n*-SMe** are reproduced from the previous work.[12] **Dithiane** and **C222-SMe** are below the fit conductance decay line for the alkane. (e) Optimized Au–molecule–Au junction structures of **C2-SMe**, **dithiane**, and **C222-SMe**. (f) Calculated transmissions of Au–molecule–Au junctions plotted against energy relative to Fermi energy, showing anti-resonance around Fermi energy for **dithiane**.

conductance than the fully extended alkane junctions. We attribute the lower-conducting longer junctions to the equatorial–equatorial configuration and focus the rest of this discussion to this junction which has a conductance of $4.1 \times 10^{-4}\ G_0$.

We next compare the experimental conductances of **C2-SMe**, **dithiane**, and **C222-SMe** with those of a series of thiomethyl-terminated linear alkanes, plotted against calculated S–S distance in Fig. 2d. Synthesis and measurements of **C*n*-SMe** was reported in ref. 12. The conductance of longest conformation of **dithiane** is significantly lower than that of linear thiomethyl-functionalized alkanes of the same length. By extrapolating the conductance decay trend of the alkanes we see that **dithiane** is more than an order of magnitude lower in conductance.

Compared with the previously studied methylthiomethyl-functionalized bicyclo[2.2.2]octane (**C222-SMe**),[10] the conductance is in the same low range as **C222-SMe** at $1.7 \times 10^{-4}\ G_0$. However, **dithiane** is much shorter molecular length as evident in Fig. 2d.

Calculation of the Landauer transmission of the Au–molecule–Au junction shown in Fig. 2e support the experimentally observed trend. Significant suppression is evident when we compare the transmission of **dithiane** with its alkane counterpart **C2-SMe** in Fig. 2f. Again, we see an antiresonance in the transmission of **dithiane** suggesting destructive quantum interference. This is also the case for some of the shorter junction conformations, although shorter junctions inevitably have somewhat higher transmission. The transmission for all junction conformations of **dithiane** are included in Fig. S7.†

While the transmission of previously studied **C222-SMe** is also very low, the transmission function is flat around E_F and does not show a clear signature of interference.[10] We note further that **dithiane**, **piperazine**, and **C222-diaza** do not have methyl substituents unlike **C222-SMe**, and we shall explore this difference in more detail below.

Ballistic current density

We investigate the transmission suppression in **piperazine**, **C222-diaza**, and **dithiane** by computing the ballistic current density through the molecules.[33,34] The Landauer transmission and current density of **C222-diaza** and **C222-SMe** calculated in the wide-band limit are shown in Fig. 3; that of **piperazine** and **dithiane** are included in Fig. S3.† In good agreement with the transmission computed with explicit Au electrodes (Fig. 1f and 2f), **C222-diaza** has an antiresonance between the HOMO and LUMO resonances. **C222-SMe** has an antiresonance close to the LUMO resonance, which is not clear in the computations shown in Fig. 2f, where Au electrodes are explicitly included. We first examine the current density of **C222-diaza** at the Fermi energy. We plot it as three-dimensional vectors in Fig. 3b, where the arrow thickness is the vector-length, and in Fig. 3c as a heat map of current through the xy-plane in the middle of the bicyclic structure (z being the direction of the current). We see that the vector field is dominated by forward current (red) directly between the two nitrogen atoms, with a backwards ring current (blue) being formed by three contributions through the through-bond paths. In Fig. 3d, we plot the current density of **C222-diaza** at -2.0 eV, *i.e.*, an energy at the other side of the antiresonance in the transmission. A clear signature of destructive quantum interference,[28] the ring currents reverse their direction and the direct current between the nitrogen atoms is now in the backwards direction (blue).

Turning to the question of why we see sharp interference features with the absence of methyl substituents, the current density indicates that despite the structural similarity **C222-diaza** differs significantly from **C222-SMe**. While the injection will be different into the bicyclic cage, the central parts are almost identical. We have not observed the threefold symmetry of the cage-structure retained in the current before. As can be seen in Fig. 3e, the current through **C222-SMe** is injected into
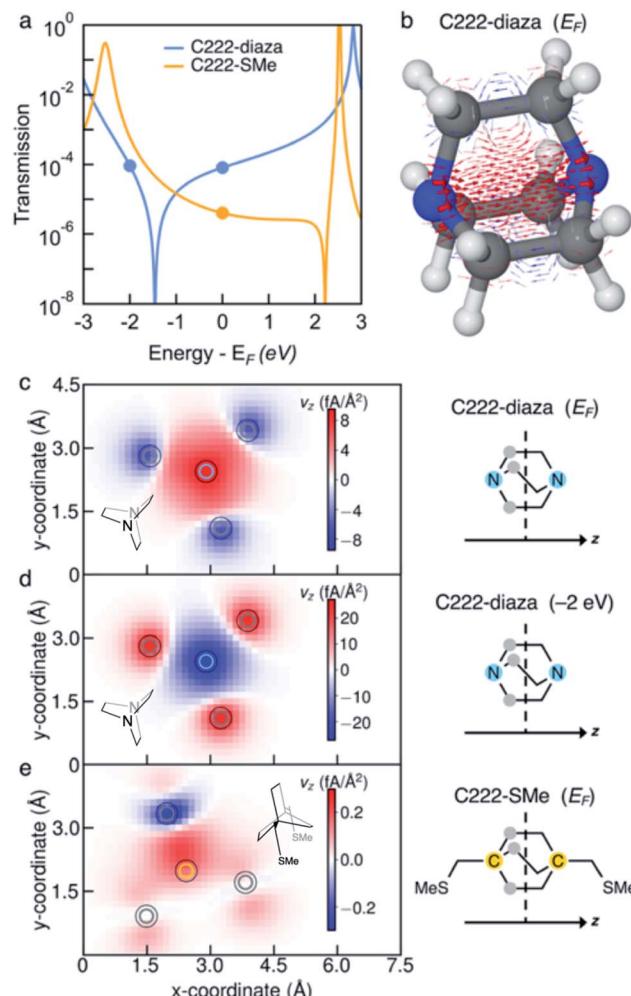
Fig. 3 (a) Transmission of **C222-diaza** and **C222-SMe** calculated with the wide-band approximation. (b) Ballistic current density in **C222-diaza** at the Fermi energy plotted as a three-dimensional vector field. Forward current is red and backwards current is blue. The arrow thickness is scaled by the vector length (the magnitude of the current density at that point in space). (c–e) Current density plotted as heat map through a cross-section at the center of the bicyclic cage for (c) **C222-diaza** at the Fermi energy, (d) **C222-diaza** at -2.0 eV and (e) **C222-SMe** at the Fermi energy. Colored circles in the heat maps mark the position of the atoms as designated in the right column.

the cage through the transoid path of the CH$_2$SMe linker,[35] and the current predominantly follows one through-bond path through the bicyclic cage. Direct current between the bridgehead carbon atoms (marked in orange) is fairly small. This analysis indicates that the strong suppression in the transmission of **C222-diaza** comes from a different balance between the through-bond and through-space paths through the molecule.[36–40] The three-fold symmetry in the current density is an indication of this different behaviour.

Furthermore, we do not see the significant substituent dependence in **C222-diaza** (Fig. S4†) that was seen in **C222-SMe**;[10] methylation in fact seems to give higher transmission in line with other saturated molecules.[41] The injection from the electrode directly into the bridgehead nitrogen atoms of
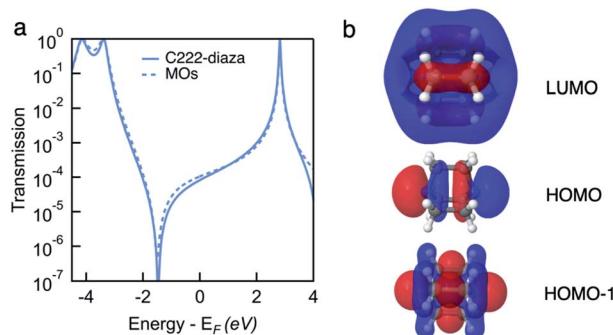
Fig. 4 (a) Transmission functions of **C222-diaza**, calculated as $T(E) = |t_{LUMO} + t_{HOMO} + t_{HOMO-1}|^2$ (dashed line) overlaid with Landauer transmission in the wide-band limit (solid). (b) MOs of **C222-diaza** calculated using DFT with B3LYP functional. White, black and blue atoms represent H, C and N, respectively.

piperazine and **C222-diaza**, and sulfur atoms of **dithiane**, thus enables the suppression of conductance in the single-molecule junctions.

To understand the interference in **C222-diaza** from a molecular orbital perspective, we reconstruct the transmission of **C222-diaza** around E_F calculated in the wide-band limit in Fig. 3 using three resonances, the LUMO, HOMO, and HOMO−1. Each resonance at an energy ε_j is coupled to the leads with a coupling γ_j. The phase factor, θ_j, describes the phase relation of the MO with respect to its overlap with either lead.[42–44]

$$t_j(E) = e^{i\theta_j} \frac{\gamma_j}{E - \varepsilon_j + i\gamma_j} \tag{1}$$

As an approximation, we use a phase factor of 0 or π depending on the symmetry of the orbital.[45]

In Fig. 4a, we see that the model transmission matches that obtained with DFT very well. The sharp antiresonance structure near E_F originates primarily from a destructive interference between the HOMO and HOMO−1 which have opposite phases ($\theta_{HOMO} - \theta_{HOMO-1} = \pi$). This can be further confirmed by looking at the calculated MOs shown in Fig. 4b. The HOMO and HOMO−1 have opposite parity at the nitrogens which couple to the leads. In the reconstructed transmission function, the HOMO and HOMO−1 are both nearly an order of magnitude better coupled to the leads than the LUMO. Therefore, the strong destructive quantum interference between HOMO and HOMO−1 can further suppress the constructive quantum interference between the HOMO and LUMO, resulting in low conductance for **C222-diaza**.[42] Analogous analyses for the other two systems are presented in the ESI.†

Conclusions

In this article we have demonstrated that the single-molecule conductance of three heterocyclic alkanes, **piperazine**, **C222-diaza** and **dithiane**, are significantly suppressed in STM-BJ experiments. Through computational analysis of the Landauer transmission and ballistic current density, we reveal that the conductance suppression is due to destructive quantum interference in the σ-system. Conclusively, we find a sharp antiresonance in the transmission near the Fermi energy, and ring currents that reverse direction at the antiresonance energy.

The measured conductance of the heterocyclic alkanes is compared to analogous linear alkanes of similar length. The conductance is suppressed in all three cases; in the case of **dithiane** the difference is over an order of magnitude. These levels of suppression have not previously been observed with any synthetically feasible carbon-based molecules. With molecular lengths around 3 Å, these heterocyclic alkanes are ultra-short molecular insulators. This finding allows us to move beyond earlier suggestions for the structural requirements for destructive σ-interference and charts a clear pathway for rational chemical design of short insulating organic molecules.

Methods

N,N′-Dimethyl-1,4-butanediamine was purchased from Ambeed. Ethylenediamine, 1,4-dithiane, 1,4-piperazine, 1,4-diazabicyclo[2.2.2]octane, *N,N,N′,N′*-tetramethyl-1,4-butanediamine and all of the solvent were purchased from Sigma Aldrich.

The molecular junction conductance was measured *via* the scanning tunneling microscope-based break junction (STM-BJ) technique at room temperature.[46,47] A sharp gold tip was driven in and out of contact with a gold substrate using 1,2,4-trichlorobenzene (TCB) as a solvent for the target molecules. One-dimensional (1D) conductance histograms are constructed using logarithmic bins (100/decade), and two-dimensional (2D) histograms use logarithmic bins along the conductance axis (100/decade) and linear bins (1000/nm) along the displacement axis, compiled from 3000–5000 traces measured at 100 mV. Junction conductance values are determined by fitting Gaussian functions without any data selection.

We analysed the experimental results by computing the Landauer transmission. All molecular geometries are optimized to local minima in vacuum to 0.01 eV Å^{-1} using density functional theory (DFT) with the PBE functional and DZP basis set as implemented in the Atomic Simulation Environment (ASE) and GPAW.[48–50] A conformational analysis is also carried out for the molecules as discussed in part 3 of the ESI.† To form Au–molecule–Au junctions, the optimized structures were placed between two four-atom Au pyramids on Au(111) surfaces and the molecular geometries were relaxed to 0.05 eV Å^{-1}. The transmission was computed at the same level of theory using the nonequilibrium Green's functions formalism as implemented in ASE.[50]

Calculation of ballistic current density was done using DFT at the same level of theory as was employed in the full transport calculations using GPAW and ASE.[48,50] Due to computational constraints, we used s-band electrodes approximated to the wide-band limit to model these single-molecule junctions. That means the gold electrodes were not explicitly included in the computation but the transmission is qualitatively similar to computations where the Au electrodes are explicitly considered.[19] The current density was calculated under an applied bias

of 1 mV. More extensive computational details of this method are included in part 4 of the ESI† and in previous works.[16,51]

Data availability

The data that support the findings of this study not included in the ESI are available from the corresponding author upon reasonable request.

Author contributions

B. Z. carried STM-BJ measurements, data analysis and molecular orbital analysis, M. H. G. carried out all the computation, L. L. measured the linear alkanes, and all authors co-wrote the manuscript.

Conflicts of interest

There are no conflicts to declare.

Acknowledgements

Notes and references

1 A. Nitzan, *Annu. Rev. Phys. Chem.*, 2001, **52**(1), 681–750.
2 J. G. Simmons, *J. Appl. Phys.*, 1963, **34**(6), 1793–1803.
3 P. Sautet and C. Joachim, *Chem. Phys. Lett.*, 1988, **153**(6), 511–516.
4 V. Rabache, J. Chaste, P. Petit, M. L. Della Rocca, P. Martin, J.-C. Lacroix, R. L. McCreery and P. Lafarge, *J. Am. Chem. Soc.*, 2013, **135**(28), 10218–10221.
5 X. Li, Z. Tan, X. Huang, J. Bai, J. Liu and W. Hong, *J. Mater. Chem. C*, 2019, **7**(41), 12790–12808.
6 C. R. Arroyo, S. Tarkuc, R. Frisenda, J. S. Seldenthuis, C. H. M. Woerde, R. Eelkema, F. C. Grozema and H. S. J. van der Zant, *Angew. Chem., Int. Ed.*, 2013, **52**(11), 3152–3155.
7 C. M. Guédon, H. Valkenier, T. Markussen, K. S. Thygesen, J. C. Hummelen and S. van der Molen, *Nat. Nanotechnol.*, 2012, **7**(5), 305–309.
8 M. Mayor, H. B. Weber, J. Reichert, M. Elbing, C. von Hänisch, D. Beckmann and M. Fischer, *Angew. Chem., Int. Ed.*, 2003, **42**(47), 5834–5838.
9 C. B. George, M. A. Ratner and J. B. Lambert, *J. Phys. Chem. A*, 2009, **113**(16), 3876–3880.
10 M. H. Garner, H. Li, M. Neupane, Q. Zou, T. Liu, T. A. Su, Z. Shangguan, D. W. Paley, F. Ng, S. Xiao, C. Nuckolls, L. Venkataraman and G. C. Solomon, *J. Am. Chem. Soc.*, 2019, **141**(39), 15471–15476.
11 H. Li, M. H. Garner, Z. Shangguan, Y. Chen, Q. Zheng, T. A. Su, M. Neupane, T. Liu, M. L. Steigerwald, F. Ng,

C. Nuckolls, S. Xiao, G. C. Solomon and L. Venkataraman, *J. Am. Chem. Soc.*, 2018, **140**(44), 15080–15088.
12 M. H. Garner, H. Li, Y. Chen, T. A. Su, Z. Shangguan, D. W. Paley, T. Liu, F. Ng, H. Li, S. Xiao, C. Nuckolls, L. Venkataraman and G. C. Solomon, *Nature*, 2018, **558**(7710), 415–419.
13 D. Q. Andrews, G. C. Solomon, R. P. Van Duyne and M. A. Ratner, *J. Am. Chem. Soc.*, 2008, **130**(51), 17309–17319.
14 T. A. Su, M. Neupane, M. L. Steigerwald, L. Venkataraman and C. Nuckolls, *Nat. Rev. Mater.*, 2016, **1**(3), 16002.
15 G. M. Locke, S. S. R. Bernhard and M. O. Senge, *Chem.–Eur. J.*, 2019, **25**(18), 4590–4647.
16 M. H. Garner and G. C. Solomon, *J. Phys. Chem. Lett.*, 2020, **11**(17), 7400–7406.
17 A. Borges, E. D. Fung, F. Ng, L. Venkataraman and G. C. Solomon, *J. Phys. Chem. Lett.*, 2016, **7**(23), 4825–4829.
18 H. Löfås, R. Emanuelsson, R. Ahuja, A. Grigoriev and H. Ottosson, *J. Phys. Chem. C*, 2013, **117**(42), 21692–21699.
19 M. H. Garner, M. Koerstz, J. H. Jensen and G. C. Solomon, *J. Phys. Chem. Lett.*, 2018, **9**(24), 6941–6947.
20 R. Emanuelsson, H. Löfås, A. Wallner, D. Nauroozi, J. Baumgartner, C. Marschner, R. Ahuja, S. Ott, A. Grigoriev and H. Ottosson, *Chem.–Eur. J.*, 2014, **20**(30), 9304–9311.
21 H. Li, M. H. Garner, Z. Shangguan, Q. Zheng, T. A. Su, M. Neupane, P. Li, A. Velian, M. L. Steigerwald, S. Xiao, C. Nuckolls, G. C. Solomon and L. Venkataraman, *Chem. Sci.*, 2016, **7**(9), 5657–5662.
22 A. K. Ismael and C. J. Lambert, *J. Mater. Chem. C*, 2019, **7**(22), 6578–6581.
23 L. Mejía, N. Renaud and I. Franco, *J. Phys. Chem. Lett.*, 2018, **9**(4), 745–750.
24 S. A. Paz, M. E. Zoloff Michoff, C. F. A. Negre, J. A. Olmos-Asar, M. M. Mariscal, C. G. Sánchez and E. P. M. Leiva, *J. Chem. Theory Comput.*, 2012, **8**(11), 4539–4545.
25 M. Paulsson, C. Krag, T. Frederiksen and M. Brandbyge, *Nano Lett.*, 2009, **9**(1), 117–121.
26 S. Martín, F. Giustiniano, W. Haiss, S. J. Higgins, R. J. Whitby and R. J. Nichols, *J. Phys. Chem. C*, 2009, **113**(43), 18884–18890.
27 C. Li, I. Pobelov, T. Wandlowski, A. Bagrets, A. Arnold and F. Evers, *J. Am. Chem. Soc.*, 2008, **130**(1), 318–326.
28 G. C. Solomon, C. Herrmann, T. Hansen, V. Mujica and M. A. Ratner, *Nat. Chem.*, 2010, **2**(3), 223–228.
29 M. Kamenetska, M. Koentopp, A. C. Whalley, Y. S. Park, M. L. Steigerwald, C. Nuckolls, M. S. Hybertsen and L. Venkataraman, *Phys. Rev. Lett.*, 2009, **102**(12), 126803.
30 I. Tamblyn, P. Darancet, S. Y. Quek, S. A. Bonev and J. B. Neaton, *Phys. Rev. B: Condens. Matter Mater. Phys.*, 2011, **84**(20), 201402.
31 T. A. Su, H. Li, M. L. Steigerwald, L. Venkataraman and C. Nuckolls, *Nat. Chem.*, 2015, **7**(3), 215–220.
32 M. Wang, Y. Wang, S. Sanvito and S. Hou, *J. Chem. Phys.*, 2017, **147**(5), 054702.
33 G. Cabra, A. Jensen and M. Galperin, *J. Chem. Phys.*, 2018, **148**(20), 204103.

34 Y. Xue and M. A. Ratner, *Phys. Rev. B: Condens. Matter Mater. Phys.*, 2004, **70**(8), 081404.

35 J. Michl and R. West, *Acc. Chem. Res.*, 2000, **33**(12), 821–823.

36 A. Borges, J. Xia, S. H. Liu, L. Venkataraman and G. C. Solomon, *Nano Lett.*, 2017, **17**(7), 4436–4442.

37 C. Jia, M. Famili, M. Carlotti, Y. Liu, P. Wang, I. M. Grace, Z. Feng, Y. Wang, Z. Zhao, M. Ding, X. Xu, C. Wang, S.-J. Lee, Y. Huang, R. C. Chiechi, C. J. Lambert and X. Duan, *Sci. Adv.*, 2018, **4**(10), eaat8237.

38 M. Carlotti, A. Kovalchuk, T. Wächter, X. Qiu, M. Zharnikov and R. C. Chiechi, *Nat. Commun.*, 2016, **7**(1), 13904.

39 D. Stefani, K. J. Weiland, M. Skripnik, C. Hsu, M. L. Perrin, M. Mayor, F. Pauly and H. S. van der Zant, *Nano Lett.*, 2018, **18**(9), 5981–5988.

40 R. Frisenda, V. A. E. C. Janssen, F. C. Grozema, H. S. J. van der Zant and N. Renaud, *Nat. Chem.*, 2016, **8**(12), 1099–1104.

41 G. Gryn'ova and C. Corminboeuf, *J. Phys. Chem. Lett.*, 2019, **10**(4), 825–830.

42 J. E. Greenwald, J. Cameron, N. J. Findlay, T. Fu, S. Gunasekaran, P. J. Skabara and L. Venkataraman, *Nat. Nanotechnol.*, 2021, **16**(3), 313–317.

43 R. Schuster, E. Buks, M. Heiblum, D. Mahalu, V. Umansky and H. Shtrikman, *Nature*, 1997, **385**(6615), 417–420.

44 G. Breit and E. Wigner, *Phys. Rev.*, 1936, **49**(7), 519–531.

45 S. Gunasekaran, J. E. Greenwald and L. Venkataraman, *Nano Lett.*, 2020, **20**(4), 2843–2848.

46 B. Xu and N. Tao, *Science*, 2003, **301**(5637), 1221–1223.

47 L. Venkataraman, J. E. Klare, I. W. Tam, C. Nuckolls, M. S. Hybertsen and M. L. Steigerwald, *Nano Lett.*, 2006, **6**(3), 458–462.

48 J. Enkovaara, C. Rostgaard, J. J. Mortensen, J. Chen, M. Dułak, L. Ferrighi, J. Gavnholt, C. Glinsvad, V. Haikola, H. A. Hansen, H. H. Kristoffersen, M. Kuisma, A. H. Larsen, L. Lehtovaara, M. Ljungberg, O. Lopez-Acevedo, P. G. Moses, J. Ojanen, T. Olsen, V. Petzold, N. A. Romero, J. Stausholm-Møller, M. Strange, G. A. Tritsaris, M. Vanin, M. Walter, B. Hammer, H. Häkkinen, G. K. H. Madsen, R. M. Nieminen, J. K. Nørskov, M. Puska, T. T. Rantala, J. Schiøtz, K. S. Thygesen and K. W. Jacobsen, *J. Phys.: Condens. Matter*, 2010, **22**(25), 253202.

49 J. P. Perdew, K. Burke and M. Ernzerhof, *Phys. Rev. Lett.*, 1996, **77**(18), 3865–3868.

50 A. Hjorth Larsen, J. Jørgen Mortensen, J. Blomqvist, I. E. Castelli, R. Christensen, M. Dułak, J. Friis, M. N. Groves, B. Hammer, C. Hargus, E. D. Hermes, P. C. Jennings, P. Bjerre Jensen, J. Kermode, J. R. Kitchin, E. Leonhard Kolsbjerg, J. Kubal, K. Kaasbjerg, S. Lysgaard, J. Bergmann Maronsson, T. Maxson, T. Olsen, L. Pastewka, A. Peterson, C. Rostgaard, J. Schiøtz, O. Schütt, M. Strange, K. S. Thygesen, T. Vegge, L. Vilhelmsen, M. Walter, Z. Zeng and K. W. Jacobsen, *J. Phys.: Condens. Matter*, 2017, **29**(27), 273002.

51 A. Jensen, M. H. Garner and G. C. Solomon, *J. Phys. Chem. C*, 2019, **123**(19), 12042–12051.